2011

Chandra Observations Of The High-Magnetic-Field Radio Pulsar J1718–3718

W. W. Zhu

V. M. Kaspi

M. A. McLaughlin

G. G. Pavlov

C.-Y. Ng

See next page for additional authors

The Astrophysical Journal, 734:44 (8pp), 2011 June 10 doi:10.1088/0004-637X/734/1/44

CHANDRA OBSERVATIONS OF THE HIGH-MAGNETIC-FIELD RADIO PULSAR J1718−3718

W. W. Zhu[1], V. M. Kaspi[1,7], M. A. McLaughlin[2,8], G. G. Pavlov[3], C.-Y. Ng[1,9],
R. N. Manchester[4], B. M. Gaensler[5], and P. M. Woods[6]
[1] Department of Physics, McGill University, Montreal, QC, H3A 2T8, Canada; zhuww@physics.mcgill.ca, vkaspi@physics.mcgill.ca, ncy@physics.mcgill.ca
[2] Department of Physics, West Virginia University, Morgantown, WV 26506, USA
[3] Department of Astronomy and Astrophysics, Pennsylvania State University, PA 16802, USA; pavlov@astro.psu.edu
[4] Commonwealth Scientific and Industrial Research Organisation Astronomy and Space Science, Australia Telescope National Facility, Epping, NSW 1710, Australia; dick.manchester@csiro.au
[5] Sydney Institute for Astronomy, School of Physics A29, The University of Sydney, NSW 2006, Australia
[6] Corvid Technologies, Huntsville, AL 35806, USA
Received 2010 November 25; accepted 2011 March 26; published 2011 May 24

ABSTRACT

High-magnetic-field pulsars represent an important class of objects for studying the relationship between magnetars and radio pulsars. Here we report on four *Chandra* observations of the high-magnetic-field pulsar J1718−3718 ($B = 7.4 \times 10^{13}$ G) taken in 2009 as well as a reanalysis of 2002 *Chandra* observations of the region. We also report an improved radio position for this pulsar based on ATCA observations. We detect X-ray pulsations at the pulsar's period in the 2009 data, with a pulsed fraction of 52% ± 13% in the 0.8–2.0 keV band. We find that the X-ray pulse is aligned with the radio pulse. The data from 2002 and 2009 show consistent spectra and fluxes: a merged overall spectrum is well fit by a blackbody of temperature 186^{+19}_{-18} eV, slightly higher than predicted by standard cooling models; however, the best-fit neutron star atmosphere model is consistent with standard cooling. We find the bolometric luminosity $L^{\infty}_{\rm bb} = 4^{+5}_{-2} \times 10^{32}$ erg s^{-1} $\sim 0.3\,\dot{E}$ for a distance of 4.5 kpc. We compile measurements of the temperatures of all X-ray-detected high-B pulsars as well as those of low-B radio pulsars and find evidence for the former being hotter on average than the latter.

Key words: pulsars: individual (PSR J1718−3718) – stars: neutron – X-rays: stars

1. INTRODUCTION

Over the past few decades, our knowledge about the neutron star family has increased significantly. Previously, only one kind of isolated neutron star was known—radio pulsars. Powered by their rotational energy, they are also called rotation-powered pulsars (RPPs). Their luminosities are generally much lower than the rotation energy loss rate, $\dot{E}$. X-ray observations have led to the discovery of several new classes of isolated neutron stars, including magnetars and X-ray-isolated neutron stars (XINSs[10]); see Kaspi (2010) for a recent review. They all exhibit distinctive properties different from those of conventional RPPs.

Magnetars are isolated, slowly rotating (known periods in the range of 2–12 s) X-ray pulsars having thermal and non-thermal X-ray luminosities that are in many cases much higher than their spin-down luminosities. Some are characterized by repeating X-ray/γ-ray bursting activity and therefore are called soft gamma repeaters (SGRs). Others are less active and are characterized by their persistent X-ray pulsations; these are classified as anomalous X-ray pulsars (AXPs). However, the distinction between these two classes has been increasingly blurred as some sources show properties of both (e.g., Gavriil et al. 2002; Kaspi et al. 2003; Woods et al. 2004; Rea et al. 2009a; Kaneko et al. 2010; Israel et al. 2010; Ng et al. 2011). They generally have very high magnetic fields ($B \sim 10^{14}$–10^{15} G), inferred by assuming that their spin-down rates are solely a result of magnetic dipole radiation. It is generally believed that their X-ray luminosities are powered by the decay of ultra-high magnetic fields (Duncan & Thompson 1992; Thompson & Duncan 1995, 1996; Thompson et al. 2002). For reviews of magnetars, see Woods & Thompson (2006), Kaspi (2007), or Mereghetti (2008).

XINSs are a small group of slowly rotating (known periods in the range of 3–11 s), nearby (distance $\leqslant$ 500 pc) neutron stars (see Kaspi et al. 2006; Haberl 2007; Turolla 2009 for reviews). Apparently emitting thermal X-ray spectra, they show no hard X-ray emission. No radio counterparts have been found for these neutron stars. Given their long periods and expected small beaming fractions, it is possible that their radio beams are misaligned with our line of sight (Kondratiev et al. 2009). Therefore, it is not clear whether or not they are intrinsically radio quiet. Timing observations of XINSs have revealed relatively high inferred magnetic fields ($\sim$ (1–3) $\times 10^{13}$ G) and spin-down ages of the order of 10^6 years (Kaplan & van Kerkwijk 2005, 2009a; Zane et al. 2005; van Kerkwijk & Kaplan 2008) for some of them. Unlike magnetars, they show no bursting activity and are much less luminous. However, their X-ray luminosities are comparable to the spin-down power of magnetars and significantly higher than those of normal RPPs of similar ages (Kaplan & van Kerkwijk 2009a). Therefore, Kaplan & van Kerkwijk (2009a) suggest that the cooling of XINSs is likely affected by magnetic-field decay heating as predicted in theory by Arras et al. (2004), Pons et al. (2007), and Aguilera et al. (2008). An alternative explanation is that the XINSs are surrounded by fallback disks and are heated due to accretion (Alpar 2007).

One likely crucial group of pulsars for understanding the relationships between RPPs, magnetars, and XINSs is the high-magnetic-field RPPs. There are now several known RPPs that have spin-down magnetic fields close to or higher than those of

[7] Canada Research Chair; Lorne Trottier Chair; R. Howard Webster Fellow of the Canadian Institute for Advanced Research (CIFAR).
[8] Also adjunct at the National Radio Astronomy Observatory, Green Bank, WV 24944, USA.
[9] Tomlinson Postdoctoral Fellow.
[10] Also known as X-ray dim isolated neutron stars (XDINSs).

Table 1
Chandra Observations of PSR J1718−3718

ObsID	Date	MJD	Frame Time (s)	Offset[a]	Live Time (ks)	R.A., Decl.[b] (deg)	N_{src}, N_{bkg}[c]	Count Rate (s^{-1})	Flux[d]
2785	2002 May 13	52407	3.24	8.′13	55.7	259.54098(8),−37.31437(6)	99, 5	0.0017(2)	9(2)
10131	2009 Feb 19	54881	0.44	0.′07	32.0	259.54098(1),−37.31419(1)	81, 0.8	0.0025(3)	8(3)
10766	2009 May 15	54966	0.44	0.′07	33.3	259.54096(1),−37.31439(1)	82, 0.6	0.0024(3)	9(2)
10767	2009 Jul 28	55040	0.44	0.′07	34.2	259.54088(1),−37.31432(1)	66, 0.9	0.0019(2)	5(2)
10768	2009 Oct 23	55127	0.44	0.′07	34.1	259.54093(1),−37.31432(1)	73, 1	0.0021(3)	7(2)

Notes.
[a] The pointing offset from PSR J1718−3718.
[b] Position of the X-ray counterpart of PSR J1718−3718 reported by the `CIAO celldetect` tool. Numbers in parentheses are 1σ uncertainties in the last quoted digit. The uncertainties listed in this column were calculated using the source detection code and are much smaller than the pointing uncertainty of *Chandra*.
[c] Total counts N_{src} and estimated background counts N_{bkg} in the source region in 0.8–2.0 keV.
[d] 0.8–2.0 keV absorbed flux in units of 10^{-15} erg s^{-1} cm^{-2}, measured from a joint fit of the spectra with N_H and kT fixed at their best-fit values.

magnetars. Some of them are radio pulsars. Sharing properties with both classes, these high-B pulsars could be transition objects between RPPs and magnetars. Indeed, some magnetars are now known to emit at radio wavelengths, and magnetar-like bursting behavior has been seen in one high-B pulsar. XTE J1810−197 is a transient AXP, first detected in outburst (Ibrahim et al. 2004). This magnetar, originally not emitting in the radio band, was observed to have radio pulsations one year after its X-ray outburst (Camilo et al. 2006). Also, the magnetar 1E 1547.0−5408 shows radio pulsations (Camilo et al. 2007). Though not a radio pulsar, the high-B rotation-powered ($B = 4.9 \times 10^{13}$ G) X-ray PSR J1846−0258 exhibited a sudden, magnetar-like X-ray outburst that lasted for a few weeks in 2006 (Gavriil et al. 2008; Kumar & Safi-Harb 2008; Ng et al. 2008). Thus, it is possible that the high-B RPPs are magnetars in quiescence. Recently, a new magnetar, PSR J1622−4950, was discovered via its active radio emission, yet it is relatively X-ray faint (Levin et al. 2010). Another magnetar, SGR 0418+5729, detected via its bursting activities, was found to have a magnetic field of $B < 8 \times 10^{12}$ G, well below that of the other magnetars, suggesting that a strong surface dipole magnetic field might not be necessary for magnetar-like behavior (van der Horst et al. 2010; Rea et al. 2010; Esposito et al. 2010). These discoveries further suggest that there could be a large, unseen population of quiescent magnetars, some of which may be "disguised" as radio pulsars.

PSR J1718−3718 is a radio pulsar discovered in the Parkes Multibeam Pulsar Survey (Hobbs et al. 2004). It has a period of $P = 3.3$ s and a spin-down rate of $\dot{P} = 1.5 \times 10^{-12}$. These imply a characteristic age of $\tau_c \equiv P/(2\dot{P}) = 34$ kyr, spin-down power $\dot{E} \equiv 4\pi^2 I \dot{P}/P^3 = 1.6 \times 10^{33}$ erg s^{-1}, where $I = 10^{45}$ g cm^2 is a fiducial moment of inertia of the pulsar, and a surface dipole magnetic field of $B \equiv 3.2 \times 10^{19}(P\dot{P})^{1/2}$ G $= 7.4 \times 10^{13}$ G, which is the second highest of all known RPPs and is higher than that of AXP 1E 2259+586[11] ($B = 5.9 \times 10^{13}$ G). PSR J1718−3718 has a dispersion measure (DM) of 373 cm^{-3} pc (Hobbs et al. 2004). Based on the DM and the NE2001 model (Cordes & Lazio 2002), the best estimated distance to the pulsar is ∼4.5 kpc. However, the NE2001 model provides a poor estimate of pulsars' distances when they are near the Galactic center (Gaensler et al. 2004). Indeed the distances estimated based on NE2001 for pulsars in nearby clusters NGC 6221 and NGC 6403 are a factor of ∼2–3 smaller than their true distances (Gaensler et al. 2008). Therefore, we suggest that the true distance of PSR J1718−3718 is probably in the range of ∼4.5–10 kpc.

An X-ray source was serendipitously detected at the radio position of PSR J1718−3718 in a 2002 *Chandra* observation. Kaspi & McLaughlin (2005) found that this X-ray source had a soft, thermal-like spectrum and therefore is the likely X-ray counterpart of the radio pulsar. However, due to the limited photon statistics (see Table 1), the spectral results were not very constraining. Also the coarse time resolution (3.24 s) in the timed exposure mode observation prevented any pulsations from being detected. Deeper *Chandra* observations with higher time resolution were proposed and conducted in 2009. Interestingly, a large period glitch occurred between 2007 September and 2009 January (R. N. Manchester & G. Hobbs 2011, in preparation). Four *Chandra* X-ray observations, each separated by ∼2 months, were taken in the hope of detecting X-ray variability, possibly associated with the glitch as occurred in the 2006 outburst of PSR J1846−0258 (e.g., Kuiper & Hermsen 2009; Livingstone et al. 2010).

Here we report on a temporal analysis of the four new *Chandra* observations of PSR J1718−3718, as well as on a spectral analysis that also includes the archival 2002 observation.

2. OBSERVATIONS AND RESULTS

Four observations of PSR J1718−3718 were taken with the *Chandra X-ray Observatory* in 2009. Each had ∼33 ks of live time (see Table 1 for details). In these observations, the pulsar was positioned on the Advanced CCD Imaging Spectrometer (ACIS; Garmire et al. 2003) S3 chip with a Y-offset of 0.′1 and a Z-offset of 0.′18 from the aim point. The other ACIS chips were turned off. The data were taken in 1/8 subarray mode (only photon events from 1/8 of the CCD were read out in this mode), in order to achieve a time resolution of 0.44 s, sufficient for timing this 3.3 s pulsar. In the 2002 observation, the pulsar was detected on the S2 chip of ACIS ∼8′ off the aim point, with a total of 99 counts in the 0.8–2.0 keV band (Table 1; Kaspi & McLaughlin 2005).

We started our analysis with the level 2 event files, which are the products of the standard reprocessing III,[12] and analyzed the data using the tools provided in `CIAO`[13] version 4.2 (`CALDB` version 4.2.0).

[11] http://www.physics.mcgill.ca/~pulsar/magnetar/main.html

[12] http://cxc.harvard.edu/ciao/repro_iii.html
[13] http://cxc.harvard.edu/ciao/

2.1. Imaging and Source Position

PSR J1718−3718 was detected in all five observations using the `celldetect` tool in `CIAO`. The best source positions as reported by `celldetect` were slightly different from one observation to another (Table 1). This is the result of the small pointing uncertainty of the *Chandra* satellite. We found the average source position to be R.A. = 17:18:09.83(1) and decl. = −37:18:51.5(2) (J2000), where the uncertainties are the standard deviation of the detected positions.

To look for extended emission, we compared the image of PSR J1718−3718 from each observation with a simulated point-source image generated by the *Chandra* Ray Tracer[14] (ChaRT, a.k.a., the *Chandra* point-spread-function (PSF) simulator) and the `MARX`[15] tool in `CIAO 4.2`. We used ChaRT to produce a collection of rays that come from a point source of the same spectrum as PSR J1718−3718 (see Section 2.2). Then we employed `MARX` to project the rays onto the detector where PSR J1718−3718 was located. For the above-mentioned images, we removed the effect of pixel randomization[16] to improve their sharpness. The PSF broadening caused by the aspect reconstruction errors and ACIS pixelization was modeled by setting the `DitherBlur` parameter to 0.″2 in `MARX`. We did not find any significant difference in the radial profile between the actual images of PSR J1718−3718 and the simulated images. We also aligned and merged all four PSR J1718−3718 images from the 2009 observations into a single image, using the `reproject_events` and `dmmerge` tools in `CIAO 4.2`. Again, no significant difference was found between the point source's radial profile in the merged image and in the simulated image. In summary, we found no evidence of extended emission in the 2009 *Chandra* observations of PSR J1718−3718.

In order to obtain a precise radio position of PSR J1718−3718, we carried out a radio imaging campaign using the Australia Telescope Compact Array (ATCA) at 20 cm and 13 cm. A 12 hr observation was made on 2007 July 9 at center frequencies of 1384 MHz and 2368 MHz, with the 6C array configuration that gives the longest baseline of 6 km. During the observation, pulsar gating was employed to record the pulsar phase information. We performed the data reduction using standard techniques in the *MIRIAD* package. After the calibration process, a usable bandwidth of 104 MHz was left for each frequency band, which was split into 13 × 8 MHz channels. We then employed the task `psrfix` to de-disperse the pulsar signals and divided the data into 16 pulsar phase bins to form individual intensity maps separately. Our final maps have restoring beams of FWHM 6.″2 × 10.″4 and 3.″2 × 5.″7 in the 20 cm and 13 cm wavebands, with corresponding rms noise of 0.5 mJy beam^{-1} and 0.6 mJy beam^{-1}, respectively. These are higher than the theoretical noise levels due to the sidelobes of the bright supernova remnant G349.7+0.2 at 8′ to the south. The pulsar is clearly detected at the >6σ level in the 20 cm waveband (Figure 1), but not at 13 cm. Finally, we employed the task `imfit` to determine the pulsar position and found R.A. = 17:18:09.84(5) and decl. = −37:18:52.3(1.4) (J2000), with a flux density 3.5 ± 0.8 mJy in one phase bin (corresponding to a mean flux density of 0.22 ± 0.05 mJy). This flux density is consistent with that in the ATNF catalog[17] for pulsars. This new radio position and the average *Chandra* X-ray position are only ∼0.″8 apart, i.e., consistent with each other.

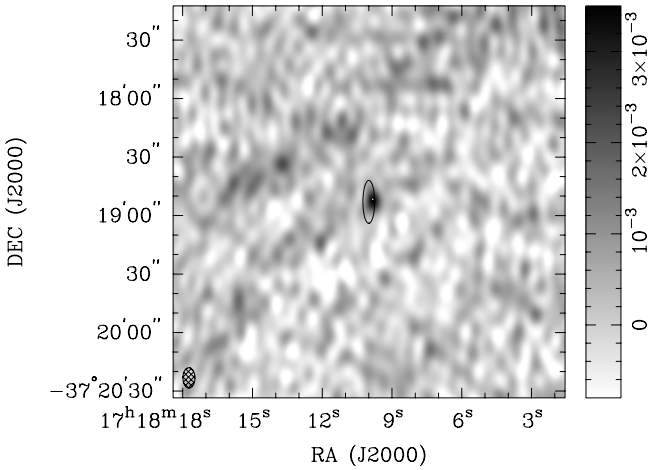

Figure 1. ATCA radio image of PSR J1718−3718 at 20 cm showing the pulsar at its "on" phase and overlaid with the 2σ error ellipse from the Parkes radio timing position (R. N. Manchester & G. Hobbs 2011, in preparation). The gray scale of the map is linear, ranging from −0.8 mJy beam^{-1} to +3.5 mJy beam^{-1} and the size of the restoring beam is shown at the lower left. The white spot marks the *Chandra* position, and its size is larger than the position uncertainty.

2.2. Spectroscopy

We extracted the spectrum of the pulsar from all five observations using the `psextract` script of `CIAO` 4.2. For the 2009 observations, we used a source region of radius 3″. A source region of radius 9.″8 was used for the 2002 observation because the source was offset from the center of the field of view where the PSF is broader. The background spectra were extracted from four circular regions of radius 10″ centered around the pulsar for all the observations. The resulting source and background spectra were then combined with RMF and ARF files generated using `psextract` and grouped with a minimum of 15 counts bin^{-1}. We found that the spectra of the pulsar are soft with very few counts above 2.0 keV. Thus for the following spectral analysis we used only the 0.8–2.0 keV band.

We fitted the five spectra separately with an absorbed blackbody model using `Xspec`[18] version 12.5.0. In each source spectrum, there are 66–99 total counts in the 0.8–2.0 keV band (Table 1), so the best-fit model parameters could not be well constrained when fitting one spectrum at a time. We fitted all five spectra jointly with a single blackbody model and found a good fit with a reduced χ^2 of 0.97 for 16 degrees of freedom. In a second joint fit, we allowed the normalization parameter to vary from observation to observation while fixing $N_{\rm H}$ and kT^{∞} at their best-fit values and found that the inferred 0.8–2.0 keV absorbed fluxes were consistent with being constant (Table 1). This suggests that there are no statistically significant spectral or flux variations from observation to observation. Based on the 0.8–2 keV absorbed fluxes, we estimate a 3σ upper limit of 60% on any flux variations.

Because the individual spectra have very few spectral bins after grouping, hence poor spectral resolution, they cannot constrain the model parameters well. In order to mitigate this problem, we summed the five spectra into a single spectrum. The resulting summed spectrum was grouped with a minimum of 20 photons bin^{-1} and had 18 spectral bins in the 0.8–2.0 keV

[14] http://cxc.harvard.edu/chart/
[15] http://space.mit.edu/CXC/MARX/
[16] http://cxc.harvard.edu/ciao/why/acispixrand.html
[17] http://www.atnf.csiro.au/research/pulsar/psrcat/
[18] http://heasarc.nasa.gov/docs/xanadu/xspec/

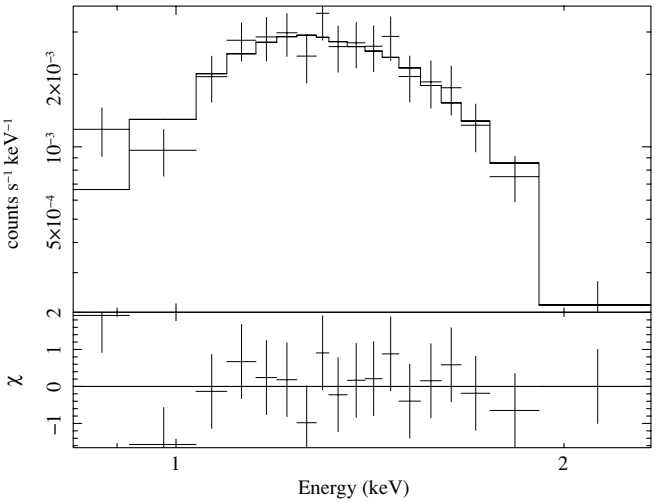

Figure 2. Summed *Chandra* ACIS spectrum of all five observations of PSR J1718−3718. The spectra are binned to contain a minimum of 20 counts bin^{-1}. The solid curve is the best-fit absorbed blackbody model. The χ in the bottom plot is defined as the difference between the value of the spectral bin and the model prediction, divided by the uncertainty of the spectral bin.

band. The spectral resolution of the summed spectrum is much better than those of the individual spectra.

We fitted the summed spectrum with a blackbody model, neutron star atmosphere (NSA) model (Zavlin et al. 1996; Pavlov et al. 1995), and a power-law model using the `wabs` model for interstellar absorption. Figure 2 shows a plot of the summed spectrum with the best-fit absorbed blackbody model.

We found a best-fit blackbody temperature of 186^{+19}_{-18} eV, corresponding to a blackbody radius of $1.8^{+1.7}_{-0.5} d_{4.5}$ km and a bolometric luminosity of $4^{+5}_{-2} \times 10^{32} d^2_{4.5}$ erg s^{-1} (assuming a fiducial distance d of 4.5 kpc). In order to explore the confidence range of the redshifted temperature kT^∞ and radius $R^\infty_{\rm bb}$ for the blackbody model, we plotted their confidence contours in the left panel of Figure 3. This indicates the lowest possible kT^∞ of 140 eV, corresponding to $R^\infty_{\rm bb} \approx 10$ km and $L^\infty_{\rm bol} \approx 5 \times 10^{33}$ erg s^{-1} (higher than the $\dot{E} = 1.6 \times 10^{33}$ erg s^{-1} of the pulsar).

The NSA model assumes that the X-ray emission of the pulsar comes from its entire surface. The best-fit local surface temperature kT is only 75^{+16}_{-10} eV ($kT^\infty = 57^{+12}_{-7}$ eV as seen from Earth), with a best-fit distance of $1.2^{+1.4}_{-0.7}$ kpc (much smaller than the estimated range of 4.5–10 kpc) assuming that the neutron star has a mass of 1.4 $M_\odot$ and a local radius of 10 km. The best-fit parameters of the blackbody and NSA models are listed in Table 2. The highly magnetized NSA model assumes a B field of 10^{13} G, less than the inferred B of 7.4×10^{13} G for PSR J1718−3718. We allowed the normalization parameter, which corresponds to $1/d^2$ where d is the distance of the neutron star, to vary when fitting the spectrum. We plotted the confidence contours of the redshifted effective surface temperature kT^∞ and distance in the right panel of Figure 3. Assuming the pulsar is at a distance between 4.5 kpc and 10 kpc, it should have a surface temperature between 75 eV and 97 eV and a bolometric luminosity $\gtrsim 10^{33}$ erg s^{-1}.

The best-fit absorbed power-law model has an unreasonably large photon index (>8); therefore, we consider it no further. We also tried to fit the 0.8–10.0 keV summed spectrum with a resonant cyclotron scattering model (Rea et al. 2008), but did not find a good fit (best reduced $\chi^2 = 2.4$ for 15 degrees of freedom); this is likely due to the lack of hard photon events in the source spectrum.

Table 2
Spectral Models for PSR J1718−3718 and Their Best-fit Parameters

Parameters	Blackbody	Hydrogen Atmosphere[a]
$N_{\rm H}$ (10^{22} cm^{-2})	1.3 ± 0.2	$1.7^{+0.1}_{-0.2}$
kT^∞ (eV)	186^{+19}_{-18}	57^{+12}_{-7}
R^∞ (km)	$1.8^{+1.7}_{-0.5} d_{4.5}$	13 (fixed)
Distance[b] (kpc)	...	$1.2^{+1.4}_{-0.7}$
$f_{\rm abs}$[c] (10^{-13} erg s^{-1} cm^{-2})	0.078 ± 0.004	0.077 ± 0.004
$f_{\rm unabs}$[d] (10^{-13} erg s^{-1} cm^{-2})	$0.7^{+0.4}_{-0.2}$	0.80 ± 0.04
L_X[e] (10^{32} erg s^{-1})	$4^{+5}_{-2} d^2_{4.5}$	2^{+3}_{-1}
$\chi^2_\nu(\nu)$	0.7(15)	0.7(15)

Notes.
[a] The NSA model for a pulsar with $B = 10^{13}$ G and a pure hydrogen atmosphere. The values of neutron star surface temperature and radius $R = 10$ km were redshifted for observers at infinite distance according to $T^\infty = T(1-2GM/Rc^2)^{1/2}$ and $R^\infty = R(1-2GM/Rc^2)^{-1/2}$ with M fixed at 1.4 $M_\odot$.
[b] In the blackbody fit, a fiducial distance d of 4.5 kpc is used as a scaling factor for the best-fit parameters. In the NSA fit, distance is fitted.
[c] Absorbed X-ray flux in 0.8–2.0 keV.
[d] Unabsorbed X-ray flux in 0.8–2.0 keV.
[e] Bolometric luminosity. For the NSA model, it is calculated based only on the pulsar's best-fit surface temperature and does not depend on distance. However, the best-fit distance in this fit is unreasonably small. If a more reasonable distance were assumed, the resulting best-fit temperature would likely become larger and thus imply a higher bolometric luminosity.

2.3. Variability and Pulse Profile

We adjusted the time stamps of the source events from all five observations to the solar system barycenter time using the `axbary` tool in `CIAO`. We binned the photon events of energy between 0.8 and 2.0 keV from the five observations evenly in time with 3.4 hr bin^{-1}. The resulting count rates were consistent with being constant with a 3σ upper limit of 48% on variations, therefore showing no evidence of significant variability on timescales of three to nine hours. In order to look for variability on shorter timescales, we measured the intervals between the arrival times of every two photons in each observation. We found that they are consistent with the exponential distribution expected from a constant count rate, and therefore show no evidence of flux variations.

Unlike the 2002 normal timed exposure mode observation that has a time resolution of 3.24 s, the four later 1/8 subarray observations have a 0.44 s time resolution (Table 1) and therefore could be used to search for pulsations from this 3.3 s pulsar. We folded the events with energies between 0.8 and 2.0 keV from the 2009 observations into eight phase bins based on a timing ephemeris obtained using the Parkes telescope (R. N. Manchester & G. Hobbs 2011, in preparation). The resulting pulse profile is shown in Figure 4. Significant pulsations were detected. We found the H test (de Jager 1994) value of the summed profile is 44.5 and the best-fit reduced χ^2 is 7.0 for 7 degrees of freedom. Both correspond to null-hypothesis possibilities of $\sim 2 \times 10^{-8}$, clearly excluding the null hypothesis. We also measured an area pulsed fraction (the fractional counts above the minimum; Gonzalez et al. 2010) of 52% ± 13% in the 0.8–2.0 keV band and a maximum–minimum pulsed fraction $(N_{\rm max} - N_{\rm min})/(N_{\rm max} + N_{\rm min})$ of 60% ± 13%.

In Figure 4, we also plotted the folded pulse profiles from individual observations. Not all of them were significantly

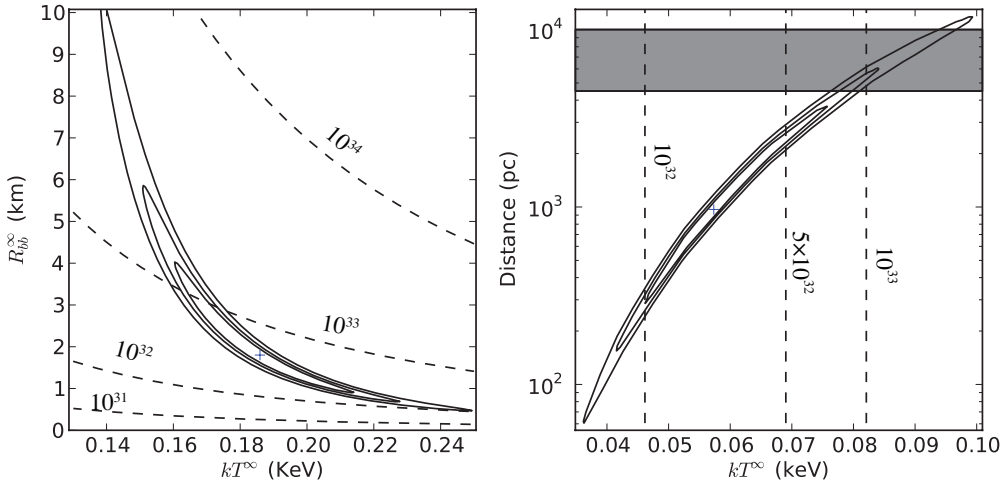

Figure 3. Left panel: 68%, 90%, and 99% confidence contours of $R_{\rm bb}^{\infty}$ (assuming a fiducial distance of 4.5 kpc) and kT^{∞} from blackbody fitting. Right panel: confidence contours of pulsar distance and kT^{∞} from fitting with an NSA model with $B = 10^{13}$ G, assuming a neutron star radius of $R = 10$ km ($R^{\infty} = 13$ km). The dashed lines in both panels are the contours of constant bolometric luminosity in units of erg s^{-1}. The shaded area in the right panel marks the region for which the pulsar's distance is 4.5–10 kpc.

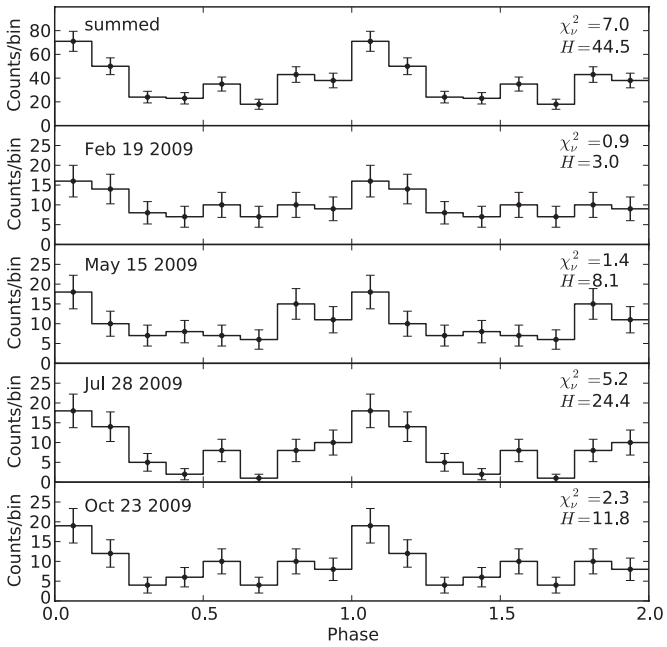

Figure 4. Pulse profiles for PSR J1718−3718 in the 0.8–2.0 keV energy range. Also given are the reduced χ^2 values for 7 degrees of freedom from fitting the profile with a constant. The peak of the pulsar's radio pulse aligns with zero phase in this plot.

pulsed. For instance, when fitted with a constant, the pulse profile of the 2009 February 19 observation gives a best-fit reduced χ^2 of 0.9 for 7 degrees of freedom and an H value of 3, neither of which excludes the null hypothesis (Table 3). Through numerical simulations, we have verified that with only 81 counts and assuming Poisson noise, it is possible for a source having a 52% pulsed fraction to produce a pulse profile of such low significance. We simulated 10,000 pulse profiles with a source with an area pulsed fraction of 52% and found that 209 of them show lower pulse significance than in the February 19 observation. Thus, even if the pulsar's profile did not change between 2009 February 19 and July 28, there is ∼2% chance of observing a pulse profile similar to the February 19 one. Taking the number of trials into account, the low pulse significance of this observation does not provide strong evidence for a change in the pulsed fraction.

Table 3
Significance of the X-Ray Pulsations of PSR J1718−3718

Observation	χ^2_7	$P_{\rm null}^{\chi^2}$	H value	$P_{\rm null}^{H}$
Summed	49.0	2×10^{-8}	44.5	2×10^{-8}
2009 Feb 19	6.2	0.5	3.0	0.3
2009 May 15	10.1	0.2	8.1	0.04
2009 Jul 28	36.6	6×10^{-6}	24.4	6×10^{-5}
2009 Oct 23	16.2	0.02	11.8	0.009

We fitted the X-ray pulse profile with a sinusoidal function to find its peak phase and compared it with that of the radio pulse after correcting for the effect of dispersion due to the interstellar medium. The radio pulse leads the X-ray pulse by 0.01 ± 0.03 in phase. Thus, they are consistent with being aligned.

3. DISCUSSION

We have reported on four new *Chandra* observations, plus a reanalysis of one archival observation, of the young, high-B RPP PSR J1718−3718. We found no evidence of magnetar-like flux variability in PSR J1718−3718 from our *Chandra* observations and set a 3σ upper limit on any flux variability of 60% in the 0.8–2 keV band. However, the possibility that a magnetar-like outburst, such as that observed from PSR J1846−0258 in 2006 which lasted for only few weeks, happened in the span of our observations cannot be ruled out.

PSR J1718−3718 's X-ray spectrum is soft and thermal and is well fit by a blackbody model. Fitting its summed spectrum with a blackbody model, we found a high-blackbody temperature of 186^{+19}_{-18} eV (Table 2) and a corresponding best-fit blackbody radius of $1.8^{+1.7}_{-0.5} d_{4.5}$ km. Such an emission radius is consistent with radiation from hot spots. However, it is not consistent with polar caps heated by return currents because of the unusually high X-ray efficiency ($L_{\rm bb}^{\infty}/\dot{E} = 0.3 d_{4.5}^2$). By contrast, models for polar-cap heating predict that no more than $\sim 10^{-3}$ of the spin-down luminosity should be converted to thermal radiation (Harding & Muslimov 2001). Note that if the distance is larger than 4.5 kpc, this conclusion is only strengthened. Indeed, at 10 kpc, $L_{\rm bb}^{\infty} > \dot{E}$. Based on the confidence contours of kT^{∞} and $R_{\rm bb}^{\infty}$ (left panel of Figure 3), we cannot completely exclude

Table 4
Surface Temperatures Measured for High-B Pulsars, Normal Pulsars, and XINSs

PSR	τ_c (kyr)	B (G)	$kT_{\rm bb}^{\infty}$ (eV)	$R_{\rm bb}^{\infty}$ (km)[D(kpc)]	$L_{\rm bb}^{\infty}/\dot{E}$[a]	References
B0950+08	18000	2.4×10^{11}	<41.0	10[0.3]	<0.06	Becker et al. (2004)
B1929+10[c]	3100	5.2×10^{11}	300^{+20}_{-30}	$0.033^{+0.006}_{-0.005}$[0.4]	3×10^{-4}	Misanovic et al. (2008)
J0538+2817	40	7.3×10^{11}	181 ± 3	2.23 ± 0.01[1.5]	0.01	Ng et al. (2007)
B0355+54[c]	564	8.4×10^{11}	200^{+96}_{-70}	$0.12^{+0.16}_{-0.07}$[1.0]	7×10^{-5}	McGowan et al. (2007)
B0823+26	4900	9.6×10^{11}	<43.0	10[0.3]	<0.10	Becker et al. (2004)
B1055−52	535	1.1×10^{12}	68 ± 3	$12.3^{+1.5}_{-0.7}$[0.8]	0.01	De Luca et al. (2005)
J0633+1746	342	1.6×10^{12}	41.4 ± 0.1	9 ± 1[0.2]	9×10^{-4}	De Luca et al. (2005)
J1811−1925	23	1.7×10^{12}	<150	10[5.0]	<0.001	Kaspi et al. (2006)
J1740+1000	114	1.8×10^{12}	70^{+10}_{-20}	7.0[1.4]	7×10^{-4}	Z. Misanovic et al. (2011, in preparation)
B1823−13	21	2.8×10^{12}	97^{+4}_{-5}	6.3[4.0]	2×10^{-4}	Pavlov et al. (2008)
B1706−44	18	3.1×10^{12}	143 ± 14	3.6 ± 0.9[2.5]	2×10^{-4}	Gotthelf et al. (2002)
B0833−45	11	3.4×10^{12}	93 ± 3	$5.1^{+0.4}_{-0.3}$[0.3]	4×10^{-5}	Manzali et al. (2007)
B1046−58	20	3.5×10^{12}	<95.0	10[2.7]	$<5 \times 10^{-4}$	Gonzalez et al. (2006)
J0205+6449	2.4	3.6×10^{12}	112 ± 9	11[3.2]	9×10^{-5}	Slane et al. (2004)
B0531+21	0.96	3.8×10^{12}	<172	16[1.7]	$<6 \times 10^{-5}$	Weisskopf et al. (2004)
B0656+14	111	4.7×10^{12}	56.0 ± 0.9	21^{+3}_{-4}[0.3]	0.01	De Luca et al. (2005)
J1357−6429[c]	7.3	7.8×10^{12}	160^{+40}_{-30}	1.0[4.1]	3×10^{-5}	C. Chang et al. (2011, in preparation)
B2334+61	41	9.9×10^{12}	109 ± 35	1.7[3.1]	8×10^{-4}	McGowan et al. (2006)
J1856−3754[b]	3800	1.5×10^{13}	63.5 ± 0.2	6.2 ± 0.1[0.2]	24	Burwitz et al. (2003)
B1916+14	88	1.6×10^{13}	130^{+100}_{-50}	0.8 ± 0.1[2.1]	0.005	Zhu et al. (2009)
J2143+0654[b]	3700	2.0×10^{13}	104 ± 4	3.1[0.4]	76	Kaplan & van Kerkwijk (2009b)
B0154+61	197	2.1×10^{13}	<73.0	10[1.7]	<0.6	Gonzalez et al. (2004)
J0720−3125[b]	1900	2.5×10^{13}	90 ± 4	6.4[0.4]	73	Haberl et al. (2006)
J0806−4123[b]	3300	2.5×10^{13}	87 ± 11	1.3[0.2]	8	Kaplan & van Kerkwijk (2009a)
J0847−4316	790	2.7×10^{13}	<100	10[3.4]	<58	Kaplan et al. (2009)
J1846−0257	442	2.7×10^{13}	<120	10[5.2]	<38	Kaplan et al. (2009)
J1308+2127[b]	1500	3.4×10^{13}	100 ± 2	4.1[0.5]	54	Schwope et al. (2007)
J1119−6127	1.8	4.1×10^{13}	210 ± 10	2.7 ± 0.7[8.4]	8×10^{-4}	Safi-Harb & Kumar (2008)
J0420−5022[b]	109	4.2×10^{13}	45 ± 3	3.3[0.3]	0.01	Haberl et al. (2004)
J1846−0258	0.88	4.9×10^{13}	<250	2.7[6.0]	$<5 \times 10^{-4}$	Livingstone et al. (2011)
J1819−1458	117	5.0×10^{13}	120 ± 20	2.1 ± 0.4[3.6]	0.4	Rea et al. (2009b)
J1734−3333	8.1	5.2×10^{13}	250^{+130}_{-80}	1^{+3}_{-1}[6.1]	0.01	Olausen et al. (2010)
J1814−1744	85	5.5×10^{13}	...	...	...	Pivovaroff et al. (2000)
J1718−3718	34	7.4×10^{13}	189^{+15}_{-22}	$1.8^{+1.7}_{-0.6}$[4.5]	0.3	This work
J1847−0130	83	9.4×10^{13}	...	...	...	McLaughlin et al. (2003)

Notes.
[a] Ratio of the pulsar's bolometric luminosity ($L_{\rm bb}^{\infty} \equiv 1.28 \times 10^{35} (R_{\rm bb}^{\infty})^2 (kT)^4$ erg s^{-1}) to spin-down power ($\dot{E}$).
[b] XINSs.
[c] These pulsars have very small blackbody radii of $R_{\rm bb}^{\infty} \leqslant 1$ km and $L_{\rm bb}^{\infty}/\dot{E} \leqslant 10^{-3}$. Their thermal radiation is likely coming from hot spots caused by return-current heating. Therefore, they are not included in Figure 5.

a blackbody fit of $kT^{\infty} = 140$ eV and $R_{\rm bb}^{\infty} = 10 d_{4.5}$ km. However, the measured 52% ± 13% area pulsed fraction suggests that the surface temperature of the pulsar cannot be uniform. Given the pulsar's spin-down age of 34 kyr, a surface temperature of 140 eV is still higher than what one would expect from a minimum cooling model for the neutron star surface without considering the effects of the magnetic field (60–90 eV; Page et al. 2006). Interestingly, the 186 eV best-fit blackbody temperature is similar to those found for the high-B PSRs J1119−6127, J1734−3333, and J1819−1458 (see Table 4 for details and references), and the transient AXP XTE J1810−197 when it was in quiescence between 1980 and 1993 (Gotthelf et al. 2004; $kT^{\infty} = 180 \pm 10$ eV).

On the other hand, fitting the spectrum with an NSA model leads to a best-estimate surface temperature of 75–97 eV (assuming a neutron star mass of 1.4 $M_{\odot}$, a local radius of 10 km, and a pulsar distance of 4.5–10 kpc), consistent with standard cooling. We note, however, that the magnetic-field strength assumed in the NSA model is 10^{13} G, almost one order of magnitude smaller than the spin-down-inferred value. Therefore, the results of the NSA model fit should be taken with caution.

Attempting to explain the X-ray thermal emission observed from magnetars, XINSs, and some high-B pulsars, Arras et al. (2004), Pons et al. (2007), and Aguilera et al. (2008) constructed neutron star cooling models in which pulsars with magnetic fields higher than 10^{13} G are significantly heated by field decay. The key evidence to support this theory is an intriguing possible correlation found between the pulsar's blackbody temperature T and spin-down magnetic field B ($T \propto B^{1/2}$) based on a sample of magnetars, XINSs, and some RPPs (Pons et al. 2007). However, their analysis did not consider high-B RPPs. Searches for evidence of magnetic-field-decay heating have been conducted on several high-B pulsars, e.g., PSRs J1814−1744 (Pivovaroff et al. 2000), J1847−0130 (McLaughlin et al. 2003), B0154+61 (Gonzalez et al. 2004), J1119−6127 (Gonzalez et al. 2005), J1718−3718 (Kaspi & McLaughlin 2005), B1916+14 (Zhu et al. 2009), and J1734−3333 (Olausen et al. 2010), and X-ray counterparts were found in some cases. Their spectra, however, have not yet been sufficiently well constrained to prove the

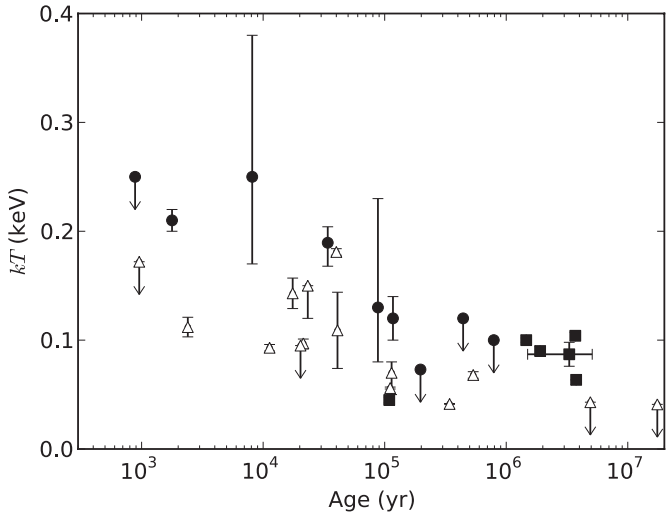

Figure 5. Blackbody temperatures vs. characteristic ages ($P/(\dot{P}(n-1))$, where n is the measured braking index, assuming $n = 3$ if it is not measured) of high-B pulsars (filled circles), normal pulsars (open triangles), and XINSs (filled squares). References are listed in Table 4.

existence of significant magnetic-field-decay heating. For a recent review on high-magnetic-field pulsars, see Ng & Kaspi (2010).

With our new data and spectral analysis of PSR J1718−3718, we are unable to confirm that it is heated by magnetic-field decay. This is mainly because the non-magnetized neutron star cooling models predict a large range of surface temperatures for a given pulsar age. However, we can compare the surface temperatures of several high-B RPPs with those of normal RPPs, provided that the temperatures were measured using the same spectral model. In Figure 5, we plot blackbody kT^{∞} versus age for a collection of pulsars including some high-B pulsars (see Table 4). From this plot, one can see that the blackbody temperatures of the high-B pulsars appear to be higher in general than those of the normal pulsars.

We also looked for the same $T - B$ correlation showed by Pons et al. (2007) in a kT^{∞} versus B plot, but the temperatures of the pulsars are too scattered to discern a trend. This could be because our sample has a small range of B but a large range of ages.

Note that three pulsars listed in Table 4 (PSRs B1929+10, B0355+54, and J1357−6449) are not plotted in Figure 4. This is because they all exhibit a large kT^{∞} with a very small blackbody radius, $R_{\rm bb}^{\infty} \lesssim 1$ km, consistent with return-current heating. For the other RPPs, we cannot rule out the possibility that their blackbody temperatures are also higher because of return currents, but these sources nevertheless provide interesting upper limits on any non-return-current thermal emission. On the other hand, return-current heating is unlikely to be present in the high-B PSRs and XINSs. This is because most of them, including PSR J1718−3718 ($B > 10^{13}$ G, see Table 4), have an X-ray efficiency of $L_{\rm bb}^{\infty}/\dot{E} \gtrsim 10^{-3}$. Such a high X-ray efficiency is clearly inconsistent with return-current heating (Harding & Muslimov 2001). Also note that the X-ray spectra of some pulsars, such as PSRs B1055−52, B0656+14, and J0633+1746, show evidence of thermal emission from both a hot spot and a much cooler neutron star surface; in these cases, only the $kT_{\rm bb}^{\infty}$ of the cool surface was used.

In summary, our *Chandra* observations of PSR J1718−3718 have revealed, for the first time, X-ray pulsations at the pulse period, as well as a thermal spectrum of blackbody temperature somewhat higher than for other RPPs having the same age. We have found a high bolometric-to-spin-down luminosity ratio, ∼0.3 for a distance of 4.5 kpc and higher for more realistic, larger distances. Although we cannot rule out standard passive cooling since a model fit with an NSA model yields a lower surface temperature, we have considered the possibility that PSR J1718−3718 exhibits enhanced thermal emission due to magnetic-field decay as predicted by models of magneto-thermal evolution (Arras et al. 2004; Pons et al. 2007; Aguilera et al. 2008). We have compiled similar measurements for the other high- and low-B RPPs and find a hint that those with higher B are generally hotter than low-B pulsars of the same age. However, deeper observations of high- and low-B pulsars are required to confirm this possibility.

We thank the referee for helpful suggestions. This research has made use of the *Chandra X-ray Observatory* and of software provided by the *Chandra* X-ray Center (CXC). V.M.K. receives support from an NSERC Discovery Grant, from CIFAR, from FQRNT, and holds a Canada Research Chair and the Lorne Trottier Chair in Astrophysics and Cosmology. M.A.M. is supported by the Sloan Foundation, the Research Corporation, and Smithsonian Astrophysical Observatory award GO9-0083A. The Australia Telescope, Compact Array is part of the Australia Telescope, which is funded by the Commonwealth of Australia for operation as a national facility managed by CSIRO. We thank Katherine Newton-McGee and John Reynolds for operating the ATCA. C.Y.N. is a CRAQ postdoctoral fellow. The work by G.G.P. was partially supported by NASA grant NNX09AC84G.

Facilities: CXO (ACIS), ATCA

REFERENCES

Aguilera, D. N., Pons, J. A., & Miralles, J. A. 2008, ApJ, 673, L167
Alpar, M. A. 2007, Ap&SS, 308, 133
Arras, P., Cumming, A., & Thompson, C. 2004, ApJ, 608, L49
Becker, W., Weisskopf, M. C., Tennant, A. F., Jessner, A., Dyks, J., Harding, A. K., & Zhang, S. N. 2004, ApJ, 615, 908
Burwitz, V., Haberl, F., Neuhäuser, R., Predehl, P., Trümper, J., & Zavlin, V. E. 2003, A&A, 399, 1109
Camilo, F., Ransom, S. M., Halpern, J. P., & Reynolds, J. 2007, ApJ, 666, L93
Camilo, F., Ransom, S., Halpern, J., Reynolds, J., Helfand, D., Zimmerman, N., & Sarkissian, J. 2006, Nature, 442, 892
Cordes, J. M., & Lazio, T. J. W. 2002, arXiv:astro-ph/0207156
de Jager, O. C. 1994, ApJ, 436, 239
De Luca, A., Caraveo, P. A., Mereghetti, S., Negroni, M., & Bignami, G. F. 2005, ApJ, 623, 1051
Duncan, R. C., & Thompson, C. 1992, ApJ, 392, L9
Esposito, P., et al. 2010, MNRAS, 405, 1787
Gaensler, B. M., Madsen, G. J., Chatterjee, S., & Mao, S. A. 2008, PASA, 25, 184
Gaensler, B. M., van der Swaluw, E., Camilo, F., Kaspi, V. M., Baganoff, F. K., Yusef-Zadeh, F., & Manchester, R. N. 2004, ApJ, 616, 383
Garmire, G. P., Bautz, M. W., Ford, P. G., Nousek, J. A., & Ricker, G. R. 2003, Proc. SPIE, 4851, 28
Gavriil, F. P., Gonzalez, M. E., Gotthelf, E. V., Kaspi, V. M., Livingstone, M. A., & Woods, P. M. 2008, Science, 319, 1802
Gavriil, F. P., Kaspi, V. M., & Woods, P. M. 2002, Nature, 419, 142
Gonzalez, M. E., Dib, R., Kaspi, V. M., Woods, P. M., Tam, C. R., & Gavriil, F. P. 2010, ApJ, 716, 1345
Gonzalez, M. E., Kaspi, V. M., Camilo, F., Gaensler, B. M., & Pivovaroff, M. J. 2005, ApJ, 630, 489
Gonzalez, M. E., Kaspi, V. M., Lyne, A. G., & Pivovaroff, M. J. 2004, ApJ, 610, L37
Gonzalez, M. E., Kaspi, V. M., Pivovaroff, M. J., & Gaensler, B. M. 2006, ApJ, 652, 569
Gotthelf, E. V., Halpern, J. P., Buxton, M., & Bailyn, C. 2004, ApJ, 605, 368

Gotthelf, E. V., Halpern, J. P., & Dodson, R. 2002, ApJ, 567, L125
Haberl, F. 2007, Ap&SS, 308, 181
Haberl, F., Turolla, R., de Vries, C. P., Zane, S., Vink, J., Méndez, M., & Verbunt, F. 2006, A&A, 451, L17
Haberl, F., et al. 2004, A&A, 424, 635
Harding, A. K., & Muslimov, A. G. 2001, ApJ, 556, 987
Hobbs, G., Lyne, A. G., Kramer, M., Martin, C. E., & Jordan, C. 2004, MNRAS, 353, 1311
Ibrahim, A. I., et al. 2004, ApJ, 609, L21
Israel, G. L., et al. 2010, MNRAS, 408, 1387
Kaneko, Y., et al. 2010, ApJ, 710, 1335
Kaplan, D. L., Esposito, P., Chatterjee, S., Possenti, A., McLaughlin, M. A., Camilo, F., Chakrabarty, D., & Slane, P. O. 2009, MNRAS, 400, 1445
Kaplan, D. L., & van Kerkwijk, M. H. 2005, ApJ, 628, L45
Kaplan, D. L., & van Kerkwijk, M. H. 2009a, ApJ, 705, 798
Kaplan, D. L., & van Kerkwijk, M. H. 2009b, ApJ, 692, L62
Kaspi, V. M. 2007, Ap&SS, 308, 1
Kaspi, V. M. 2010, Proc. Natl Acad. Sci., 107, 7147
Kaspi, V. M., Gavriil, F. P., Woods, P. M., Jensen, J. B., Roberts, M. S. E., & Chakrabarty, D. 2003, ApJ, 588, L93
Kaspi, V. M., & McLaughlin, M. A. 2005, ApJ, 618, L41
Kaspi, V. M., Roberts, M. S. E., & Harding, A. K. 2006, in Compact Stellar X-ray Sources, ed. W. H. G. Lewin & M. van der Klis (Cambridge: Cambridge Univ. Press), 279
Kondratiev, V. I., McLaughlin, M. A., Lorimer, D. R., Burgay, M., Possenti, A., Turolla, R., Popov, S. B., & Zane, S. 2009, ApJ, 702, 692
Kuiper, L., & Hermsen, W. 2009, A&A, 501, 1031
Kumar, H. S., & Safi-Harb, S. 2008, ApJ, 678, L43
Levin, L., et al. 2010, ApJ, 721, L33
Livingstone, M. A., Kaspi, V. M., & Gavriil, F. P. 2010, ApJ, 710, 1710
Livingstone, M. A., Ng, C.-Y., Kaspi, V. M., Gavriil, F. P., & Gotthelf, E. V. 2011, ApJ, 730, 66
Manzali, A., De Luca, A., & Caraveo, P. A. 2007, ApJ, 669, 570
McGowan, K. E., Vestrand, W. T., Kennea, J. A., Zane, S., Cropper, M., & Córdova, F. A. 2007, Ap&SS, 308, 309
McGowan, K. E., Zane, S., Cropper, M., Vestrand, W. T., & Ho, C. 2006, ApJ, 639, 377
McLaughlin, M. A., et al. 2003, ApJ, 591, L135
Mereghetti, S. 2008, A&AR, 15, 225
Misanovic, Z., Pavlov, G. G., & Garmire, G. P. 2008, ApJ, 685, 1129
Ng, C.-Y., & Kaspi, V. M. 2010, arXiv:1010.4592
Ng, C.-Y., Romani, R. W., Brisken, W. F., Chatterjee, S., & Kramer, M. 2007, ApJ, 654, 487
Ng, C.-Y., Slane, P. O., Gaensler, B. M., & Hughes, J. P. 2008, ApJ, 686, 508
Ng, C.-Y., et al. 2011, ApJ, 729, 131
Olausen, S. A., Kaspi, V. M., Lyne, A. G., & Kramer, M. 2010, ApJ, 725, 985
Page, D., Geppert, U., & Weber, F. 2006, Nucl. Phys. A, 777, 497
Pavlov, G. G., Kargaltsev, O., & Brisken, W. F. 2008, ApJ, 675, 683
Pavlov, G. G., Shibanov, Y. A., Zavlin, V. E., & Meyer, R. D. 1995, in The Lives of the Neutron Stars (NATO ASI Series), ed. A. Alpar, Ü. Kiziloğlu, & J. van Paradis (Dordrecht: Kluwer), 71
Pivovaroff, M., Kaspi, V. M., & Camilo, F. 2000, ApJ, 535, 379
Pons, J. A., Link, B., Miralles, J. A., & Geppert, U. 2007, Phys. Rev. Lett., 98, 071101
Rea, N., Zane, S., Turolla, R., Lyutikov, M., & Götz, D. 2008, ApJ, 686, 1245
Rea, N., et al. 2009a, MNRAS, 396, 2419
Rea, N., et al. 2009b, ApJ, 703, L41
Rea, N., et al. 2010, Science, 330, 944
Safi-Harb, S., & Kumar, H. S. 2008, ApJ, 684, 532
Schwope, A. D., Hambaryan, V., Haberl, F., & Motch, C. 2007, Ap&SS, 308, 619
Slane, P., Helfand, D. J., van der Swaluw, E., & Murray, S. S. 2004, ApJ, 616, 403
Thompson, C., & Duncan, R. C. 1995, MNRAS, 275, 255
Thompson, C., & Duncan, R. C. 1996, ApJ, 473, 322
Thompson, C., Lyutikov, M., & Kulkarni, S. R. 2002, ApJ, 574, 332
Turolla, R. 2009, in Neutron Stars and Pulsars, ed. W. Becker (Astrophysics and Space Science Library, Vol. 357; Berlin: Springer), 141
van der Horst, A. J., et al. 2010, ApJ, 711, L1
van Kerkwijk, M. H., & Kaplan, D. L. 2008, ApJ, 673, L163
Weisskopf, M. C., O'Dell, S. L., Paerels, F., Elsner, R. F., Becker, W., Tennant, A. F., & Schwarz, D. A. 2004, ApJ, 601, 1050
Woods, P. M., & Thompson, C. 2006, in Compact Stellar X-ray Sources, ed. W. H. G. Lewin & M. van der Klis (Cambridge: Cambridge Univ. Press), 547
Woods, P. M., et al. 2004, ApJ, 605, 378
Zane, S., Cropper, M., Turolla, R., Zampieri, L., Chieregato, M., Drake, J. J., & Treves, A. 2005, ApJ, 627, 397
Zavlin, V. E., Pavlov, G. G., & Shibanov, Y. A. 1996, A&A, 315, 141
Zhu, W., Kaspi, V. M., Gonzalez, M. E., & Lyne, A. G. 2009, ApJ, 704, 1321